Eur. Phys. J. A **17**, 29–36 (2003)
DOI 10.1140/epja/i2002-10144-3

THE EUROPEAN PHYSICAL JOURNAL A

Lifetime measurements in ^{148}Gd

Zs. Podolyák[1,a], P.G. Bizzeti[2], A.M. Bizzeti-Sona[2], S. Lunardi[3], D. Bazzacco[3], A. Dewald[4], A. Algora[5,b], G. de Angelis[5], E. Farnea[3], A. Gadea[5], D.R. Kasemann[4], T. Klug[4], Th. Kröll[3,c], S. Lenzi[3], D.R. Napoli[5], C.M. Petrache[3,d], R. Peusquens[4], C. Rossi Alvarez[3], T. Martinez[5], and C.A. Ur[3,e]

[1] Department of Physics, University of Surrey, Guildford GU2 7XH, UK
[2] Dipartimento di Fisica dell'Università and INFN, Sezione di Firenze, Firenze, Italy
[3] Dipartimento di Fisica dell'Università and INFN, Sezione di Padova, Padova, Italy
[4] Institut für Kernphysik, Universität zu Köln, Köln, Germany
[5] INFN, Laboratori Nazionali di Legnaro, Legnaro (Padova), Italy

Received: 14 November 2002 /
Published online: 29 April 2003 –
Communicated by D. Schwalm

Abstract. Lifetimes of excited states in ^{148}Gd were measured using the recoil distance method with a plunger device coupled to the EUROBALL Ge detector array. The differential decay curve method in coincidence mode allowed the unambiguous determination of lifetimes of more than 20 excited states. The obtained transition strengths are in good agreement with the shell model calculations. The effect of the $Z = 64$ subshell closure on the $B(E2 : 2^+ \rightarrow 0^+)$ reduced strengths above the $N = 82$ magic number is discussed.

PACS. 21.10.Tg Lifetimes – 21.10.Ky Electromagnetic moments – 27.60.+j $90 \leq A \leq 149$

1 Introduction

The ^{148}Gd nucleus has two neutrons more with respect to the doubly magic $^{146}_{64}$Gd, therefore it is expected that its excited states have a shell model structure. Furthermore, it is well established that the octupole collectivity plays an important role in this region of the Segrè chart [1]. The competition between the single particle and collective octupole modes of nuclear excitations has attracted particular attention, and ^{148}Gd is one of the few nuclei where a double octupole-phonon state was firmly established [2].

The normal-deformed medium- and high-spin structure of ^{148}Gd was studied extensively. The most complete level schemes were deduced by Piiparinen *et al.* from (α,4n) and (^{3}He,3n) reactions [3], and by Drigert *et al.* from the (^{36}S,4n) reaction [4]. The level structure was interpreted in terms of the spherical shell model with the 3^- octupole phonon explicitly taken into account [3].

Altough the medium- and high-spin structure is well known, with firmly assigned spins and parities, very little is known about the electromagnetic transition probabilities. Below spin $I = 20$, the lifetimes of the octupole states $(\nu f_{7/2}^2 \times 3^-)9^-$ and $(\nu f_{7/2}^2 \times 3^- \times 3^-)12^+$ were measured [5–7], and therefore the transition strengths of the γ-rays decaying from these levels were obtained. The strengths of the $2_1^+ \rightarrow 0^+$ and $3_1^- \rightarrow 0^+$ transitions were also determined in a model-dependent way from a $(\mathrm{p}, \mathrm{p}')$ experiment on radioactive ^{148}Gd target [8].

In the current article we present the results of our picosecond lifetime measurements by the recoil distance method.

2 Experiment

The level scheme of ^{148}Gd nucleus is characterised by the presence of the 9^- $\tau = 23.9$ ns yrast isomeric state [9]. In order to be able to determine the much shorter lifetimes of the levels below this nanosecond isomer, these states have to be populated by sidefeeding following particle evaporation. Therefore, a light-particle reaction had to be used. The ^{148}Gd nucleus has been populated via the ^{141}Pr(^{11}B, 4n) reaction. The beam was delivered by

[a] e-mail: Z.Podolyak@surrey.ac.uk
[b] *Permanent address*: Institute of Nuclear Research of the Hungarian Academy of Sciences, 4001 Debrecen, P.O. Box 51, Hungary.
[c] *Present address*: Technische Universität München, Garching, Germany.
[d] *Permanent address*: Dipartimento di Fisica, Università di Camerino, Italy.
[e] *Permanent address*: Institute of Physics and Nuclear Engineering, Bucharest, Romania.

the Tandem XTU accelerator of Legnaro National Laboratories. The target consisted of 0.48 mg/cm^2 ^{141}Pr on a 2.2 mg/cm^2 gold support. It was mounted with the Au support facing the beam in the Cologne plunger [10] in front of a 6 mg/cm^2 thick stretched gold stopper foil. The incident beam energy of 50.5 MeV corresponded to 49 MeV at the ^{141}Pr surface, and led to an input spin of $I \approx 15$. Data were taken at 17 stopper-target distances between 0.7 μm and 2 mm. Each flight distance up to 450 μm was controlled and regulated via a piezoelectric feedback system.

The γ-rays were detected with the EUROBALL Ge detector array [11], consisting of 15 cluster detectors (7 Ge crystals each) at backward angles, 26 clover detectors (4 Ge crystals each) around 90° and 30 tapered detectors (1 Ge crystal each) at forward angles relative to the beam direction. Events with at least four non-suppressed Ge detectors firing in coincidence were registered on tape. Energy calibration of the spectra and gain matching between the different Ge detectors have been performed using standard γ-ray sources as well as known γ-ray transitions of the nuclei populated in the reaction.

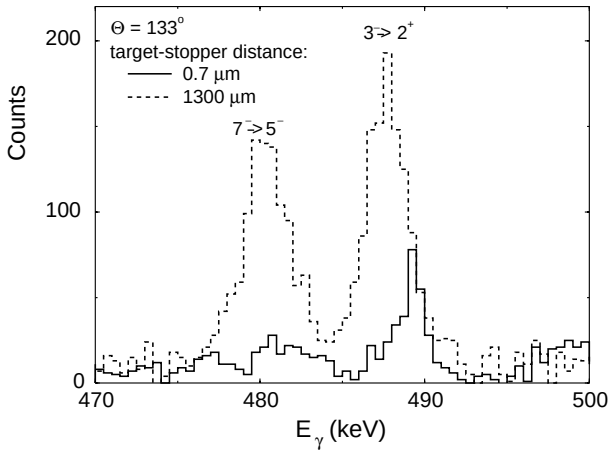

Fig. 1. Sample of gated spectra. The figure shows the 482 keV $7^- \rightarrow 5^-$ and 489 keV $3^- \rightarrow 2^+$ γ-ray transitions detected at the angle of $\theta = 133°$, for two different target-stopper distances; gated mainly (see text) on the shifted component of the 809 keV $5^- \rightarrow 3^-$ transition at $\theta = 35°$.

3 Data analysis

The Ge detectors of EUROBALL were organised into six rings at mean angles of 15°, 35°, 52°, 90°, 133° and 156°. For each target-stopper distance the Compton-suppressed three- and higher-fold events were sorted into asymmetric $\gamma\gamma$ matrices with one particular ring on each axis. The six rings correspond to 30 different combinations of rings, resulting for the 17 target-stopper distances in a total of 510 matrices.

In the analysis of the decay function the differential decay curve method (DDCM) [12,13] was used. In this technique one gates on the shifted component of the feeding transition and analyses the stopped (unshifted) and shifted parts of the depopulating transition. An example of a gated spectrum is shown in fig. 1. The lifetime of the state is given by

$$\tau = \frac{I_{\mathrm{u}}^{\mathrm{d}}}{\mathrm{d}I_{\mathrm{s}}^{\mathrm{d}}/\mathrm{d}t}\,, \qquad (1)$$

where $I_{\mathrm{u}}^{\mathrm{d}}$ and $I_{\mathrm{s}}^{\mathrm{d}}$ are the intensities of the unshifted and shifted components of the depopulating transition, and $t = d/v$ is the flight time. The above formula refers to the case when one gates on the direct feeder transition, but the DDCM can be used even by gating on (the shifted component of) an indirect feeder [13]. In this case the lifetime formula is slightly modified:

$$\tau = \frac{I_{\mathrm{u}}^{\mathrm{d}} - \alpha I_{\mathrm{u}}^{\mathrm{f}}}{\mathrm{d}I_{\mathrm{s}}^{\mathrm{d}}/\mathrm{d}t}\,, \qquad (2)$$

where $I_{\mathrm{u}}^{\mathrm{f}}$ is the unshifted component of the direct feeder and α is the ratio between the total (shifted + unshifted) intensities of the depopulating and direct feeder transitions in coincidence with the shifted indirect feeder.

The coincidence DDCM allows the determination of the lifetime of the state of interest unambiguously since the uncertainties about feeding times and intensities are avoided. To use this method, one needs fully separated stopped and Doppler-shifted components. Since in our particular case the recoil velocity is very low due to the low mass of the projectile, the two components of a peak are separated only for high-energy transitions and for rings far away from 90°. If the two components are not separated, and this is our usual case, when gating on the shifted component of the feeding transition, in order to get good statistics we could not avoid gating on a small portion of the stopped peak, too. This increases the intensity of the unshifted part of the depopulating transition, therefore a correction is needed. The increase in intensity is $\Delta I_{\mathrm{u}}^{\mathrm{d}} = (\Delta I_{\mathrm{u}}^{\mathrm{f}}/I_{\mathrm{u}}^{\mathrm{f}}) \cdot I_{\mathrm{uu}}^{\mathrm{fd}}$, where $\Delta I_{\mathrm{u}}^{\mathrm{f}}/I_{\mathrm{u}}^{\mathrm{f}}$ is the fraction of the unshifted component taken in the gate, and $I_{\mathrm{uu}}^{\mathrm{fd}}$ is the coincidence intensity of the stopped (unshifted) feeding and stopped depopulating transitions. The $I_{\mathrm{uu}}^{\mathrm{fd}}$ coincidence intensity was determined from the analysed matrix (individually for each target-stopper distance) by gating on the whole stopped depopulating transition on the second axis. The fraction of the stopped component taken in the gate, $\Delta I_{\mathrm{u}}^{\mathrm{f}}/I_{\mathrm{u}}^{\mathrm{f}}$, was determined in two different ways, leading to similar results. A spectrum presenting the unshifted populating transition is created by gating from above on the stopped part of its feeder: i) the ratio is determined directly by integrating the counts in the appropriate channels, and ii) the stopped populating peak was fitted and the peak position and their Gaussian width obtained. Then, considering the Gaussian shape of the peak, the $\Delta I_{\mathrm{u}}^{\mathrm{f}}/I_{\mathrm{u}}^{\mathrm{f}}$ ratio was calculated. This latter method works especially well when the lifetime was obtained from matrices for which the gating on the unshifted feeder was performed at a forward angle. This requires that the high-energy part of the unshifted component was caught in the gate; therefore the deviation of the shape from the

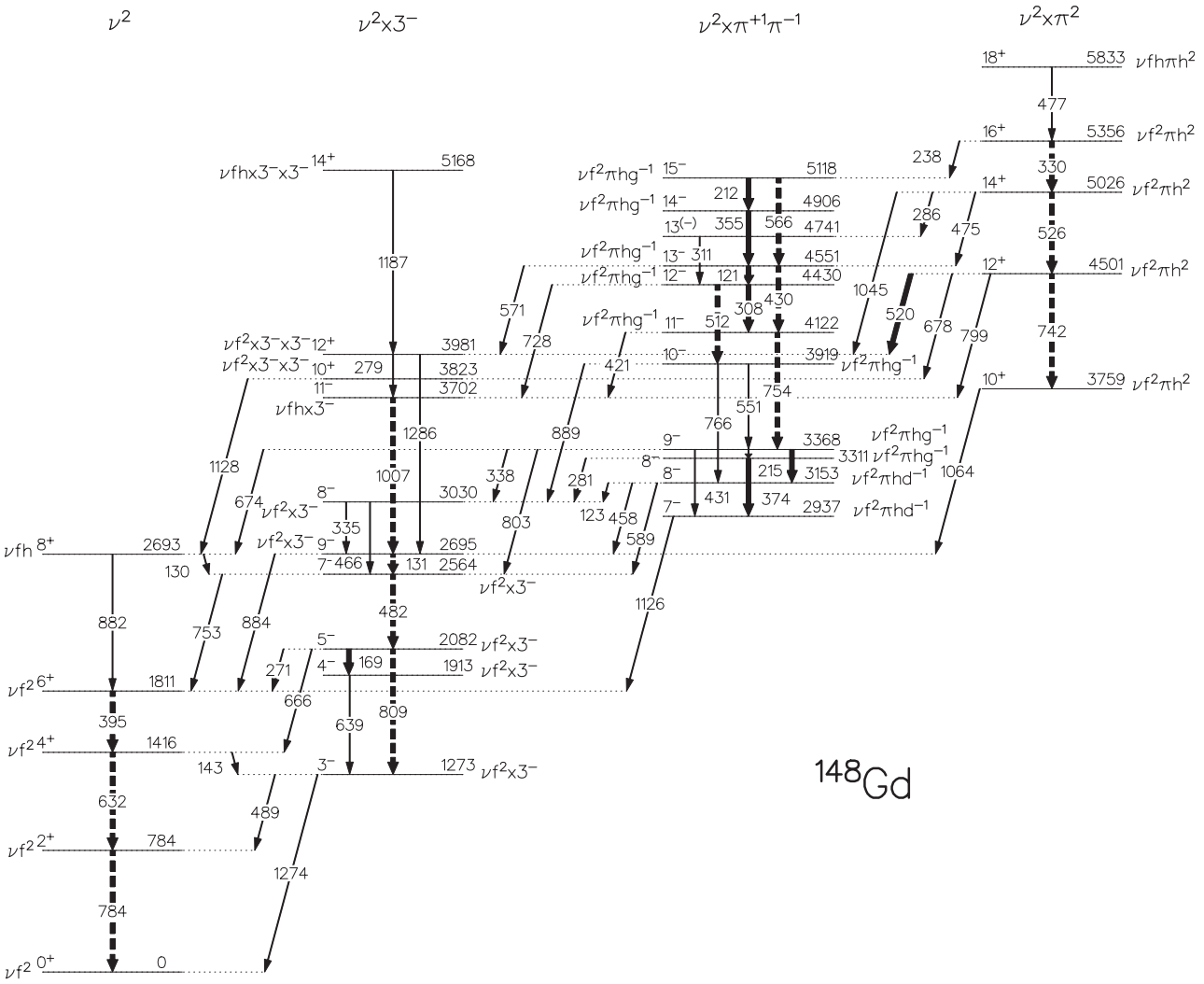

Fig. 2. Partial level scheme of ^{148}Gd. The thick dashed arrows represent strong $E2$ transitions ($B(E2) > 5$ W.u.). Similarly, the strong $M1$ transitions, $B(M1) > 10^{-2}$ W.u., are indicated by thick continuous arrows. All the other transitions are represented by thin arrows.

Gaussian distribution (because of its low-energy tail) does not affect the result.

A crucial point in the analysis of the plunger experiments is the normalisation of the data taken from different matrices, corresponding to different distances. In the first instance the matrices were normalised directly to their number of events. To check the quality of this normalisation and to correct it when necessary, we determined the coincidence intensity of the most intense γ-rays. With the final normalisation all the coincidence intensities were constant in the different matrices.

4 Results

The velocity of the recoiling nucleus was determined by using the position of the stopped and Doppler-shifted components of the strong and high-energy $E_\gamma = 1007$ keV, $11^- \rightarrow 9^-$ transition in ^{148}Gd. The obtained recoil velocity $v = 1.62(7)$ μm/ps corresponds to 0.54(2)% of the speed of light.

A partial level scheme of ^{148}Gd is shown in fig. 2. The obtained lifetimes of the excited states in ^{148}Gd as well as the transition strengths of the decaying transitions are listed in table 1. All the lifetimes, but one, are obtained from the present experiment. The lifetime of the 2995 keV 9^- isomeric state, $\tau = 23.9$ ns, is taken from the literature [9], since our plunger experiment was not sensitive for such long lifetimes. Previous to our measurement only the lifetime of the mentioned isomer and that of the 3981 keV 12^+ two-octupole phonon state were known [9]. All the other lifetimes were determined for the first time. The range of the determined lifetimes is from few picoseconds to few hundred picoseconds.

All the lifetimes presented here are the average value of those determined independently of different ring-ring combinations. The used $\gamma\gamma$ matrices depended on the individual cases as a function of statistics and contaminating

Table 1. Lifetime of excited states and reduced transiton strengths in ^{148}Gd.

E_x (keV)	τ (ps)	$I_i^\pi \to I_f^\pi$	E_γ (keV)	σL	$B(\sigma L)$ (W.u.)
784	6.0(17)	$2^+ \to 0^+$	784.4	$E2$	9.8(28)
1416	11.7(35)	$4^+ \to 2^+$	631.9	$E2$	13.9(42)
		$4^+ \to 3^-$	142.9	$E1$	$4.2(13) \times 10^{-4}$
1811	257(29)	$6^+ \to 4^+$	394.6	$E2$	6.8(8)
2693	19.0(41)	$8^+ \to 6^+$	882.4	$E2$	1.6(4)
		$8^+ \to 7^-$	129.5	$E1$	$2.8(16) \times 10^{-4}$
3759	10.9(15)	$10^+ \to 9^-$	1063.6	$E1$	$2.7(4) \times 10^{-5}$
3981	88(9)[a]	$12^+ \to 9^-$	1285.6	$E3$	66(9)
		$12^+ \to 11^-$	278.9	$E1$	$1.8(2) \times 10^{-4}$
4501	5.6(31)	$12^+ \to 11^-$	798.9	$E1$	$5.5(33) \times 10^{-6}$
		$12^+ \to 10^+$	742.1	$E2$	5.1(28)
		$12^+ \to 10^+$	677.9	$E2$	1.8(10)
		$12^+ \to 12^+$	519.9	$M1$	$2.0(11) \times 10^{-2}$
5026	36(20)	$14^+ \to 12^+$	1045.3	$E2$	0.02(1)
		$14^+ \to 12^+$	525.5	$E2$	9.6(55)
		$14^+ \to 13^-$	475.3	$E1$	$9.5(58) \times 10^{-6}$
		$14^+ \to 13^-$	285.5	$E1$	$1.7(11) \times 10^{-5}$
5356	266(38)	$16^+ \to 14^+$	329.8	$E2$	14.3(28)
		$16^+ \to 15^-$	238.0	$E1$	$9.8(20) \times 10^{-6}$
1273	50(3)	$3^- \to 0^+$	1273.5	$E3$	41(6)
		$3^- \to 2^+$	489.0	$E1$	$6.1(4) \times 10^{-5}$
2082	3.8(19)	$5^- \to 3^-$	808.7	$E2$	10.6(54)
		$5^- \to 4^+$	666.0	$E1$	$1.9(9) \times 10^{-5}$
		$5^- \to 6^+$	271.1	$E1$	$3.6(18) \times 10^{-4}$
		$5^- \to 4^-$	169.2	$M1$	$6.2(32) \times 10^{-1}$
2564	30.7(43)	$7^- \to 6^+$	752.8	$E1$	$1.1(2) \times 10^{-5}$
		$7^- \to 5^-$	481.7	$E2$	12.7(19)
2695	23900(450)[b]	$9^- \to 6^+$	883.6	$E3$	51(2)
		$9^- \to 7^-$	130.8	$E2$	5.8(2)
2937	5.5(37)	$7^- \to 6^+$	1125.6	$E1$	$4.5(30) \times 10^{-5}$
3030	75(19)	$8^- \to 7^-$	465.8	$M1$	$2.5(7) \times 10^{-3}$
		$8^- \to 9^-$	334.9	$M1$	$4.3(11) \times 10^{-3}$
3368	27.6(31)	$9^- \to 7^-$	803.4	$E2$	0.2(1)
		$9^- \to 8^+$	673.9	$E1$	$8.5(20) \times 10^{-6}$
		$9^- \to 7^-$	430.5	$E2$	1.9(7)
		$9^- \to 8^-$	337.7	$M1$	$7.9(14) \times 10^{-3}$
		$9^- \to 8^-$	214.8	$M1$	$2.8(6) \times 10^{-2}$
		$9^- \to 8^-$	57	$M1$	$1.6(6) \times 10^{-4}$
3702	1.8(57)	$11^- \to 9^-$	1006.8	$E2$	9(28)
3919	12.8(22)	$10^- \to 8^-$	888.6	$E2$	0.9(2)
		$10^- \to 8^-$	765.7	$E2$	2.6(5)
		$10^- \to 9^-$	551.0	$M1$	$2.0(4) \times 10^{-3}$
4122	6.7(49)	$11^- \to 9^-$	754.2	$E2$	10(7)
		$11^- \to 11^-$	420.6	$M1$	$3.2(26) \times 10^{-3}$
4430	17(13)	$12^- \to 11^-$	727.9	$M1$	$4.8(33) \times 10^{-4}$
		$12^- \to 10^-$	511.6	$E2$	11.4(85)
		$12^- \to 11^-$	308.4	$M1$	$2.9(22) \times 10^{-2}$
4551	55(8)	$13^- \to 12^+$	571.0	$E1$	$3.4(7) \times 10^{-6}$
		$13^- \to 11^-$	429.5	$E2$	5.0(9)
		$13^- \to 12^-$	121.3	$M1$	$1.0(2) \times 10^{-2}$
4906	4(13)	$14^- \to 13^-$	355.0	$M1$	$1.8(59) \times 10^{-1}$
5118	23.6(120)	$15^- \to 13^-$	566.4	$E2$	6.2(32)
		$15^- \to 14^-$	211.5	$M1$	$5.8(30) \times 10^{-2}$

([a]) A previous measurement [6] gave the lifetime of this state as 83(10) ps.
([b]) This lifetime is taken from the compilation of ref. [9].

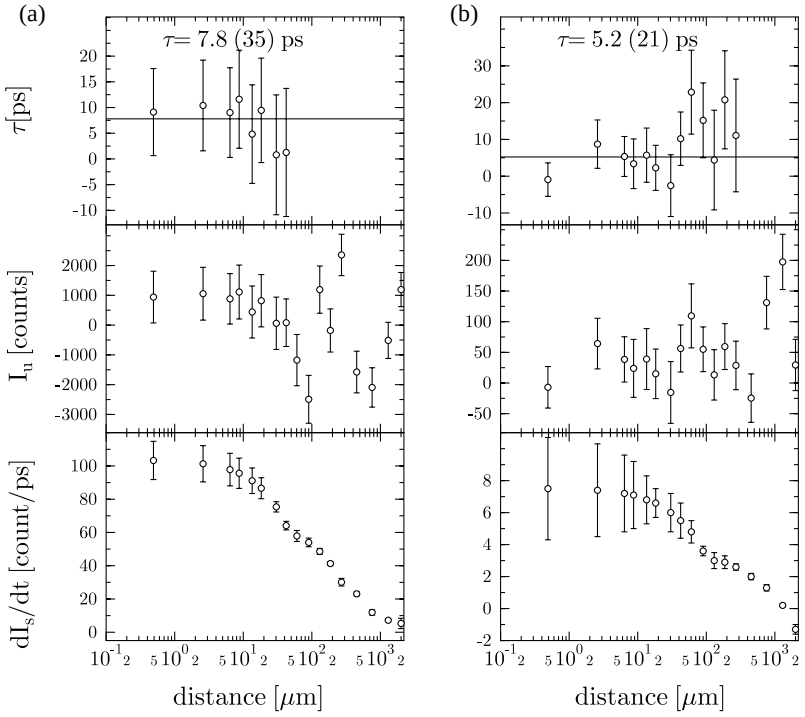

Fig. 3. Examples of lifetime analysis of the 2_1^+ state at 784 keV. For each distance, the value of the mean life (upper panel) is deduced from the intensity of the unshifted component I_u of the 784 keV transition (middle panel) and from the corresponding time derivative dI_s/dt of the shifted component (lower panel). (a) Gate on the direct feeder 632 keV $4^+ \rightarrow 2^+$ transition at 133°, analysed 784 keV at 133°; (b) gate on the 632 keV $4^+ \rightarrow 2^+$ transition at 156°, analysed 784 keV at 52°. Note that the accepted lifetime (given in table 1) is the weighted average of the lifetimes deduced from different ring-ring combinations.

transitions. Spectra obtained with gates on both direct and indirect feeding transitions were used. Correction for gating partially on the stopped feeder had to be applied in most cases. Exceptions are when gating on the shifted part of the high-energy 1126 and 1187 keV transitions feeding the 6_1^+ and 12_1^+ states. Using these gates, in addition to the lifetimes of the 6_1^+ and 12_1^+ levels, the lifetime of the 4_1^+ and 11_1^- states, populated indirectly by the mentioned high-energy transitions, were also determined. The lifetimes of the 4_1^+ and 11_1^- states obtained by using the gate on direct feeder and on the indirect feeder are in good agreement, indicating that the applied corrections for partially gating on the unshifted component were appropriate. Examples of lifetime data are shown in figs. 3 and 4.

Apart from the few particular cases, specified below, values of the branching ratios used to derive the transition strength were taken from Nuclear Data Sheets compilation [9]. We deviated from these values only in few special cases. Due to the particular interest in collective octupole transitions and the recent identification of the $3^- \rightarrow 0^+$ $E3$ transition [7], the branching ratios for the 3_1^-, 9_1^-, 12_1^+ states at energies of 1273, 2695, 3981 keV were determined from our two previous thick-target experiments described and discussed in detail in ref. [7]. The same data were used to get the branching ratio for the 3368 keV 9^- state, for which the intensity of the low-energy 57 keV transition ($B_R(\gamma + e^-) = 5.8\%$) was not given previously.

5 Discussion

5.1 Two-particle excitations

The 0^+ ground state and the yrast 2^+, 4^+, 6^+ excited states are formed by the coupling of the two $\nu f_{7/2}$ valence neutrons outside the $N = 82$ closed shell. The similar transition strengths of the $E2$ quadrupole transitions connecting them, namely $B(E2;\ 2^+ \rightarrow 0^+) = 10(3)$ W.u., $B(E2;\ 4^+ \rightarrow 2^+) = 14(4)$ W.u. $B(E2;\ 6^+ \rightarrow 4^+) = 7(1)$ W.u. indicate the same intrinsic structure for these states. Promoting one neutron into the $h_{9/2}$ orbital provides the 8^+ state at 2694 keV. As is expected, the transition strength of the $8^+ \rightarrow 6^+$ transition, 1.6(4) W.u., is much lower than the $B(E2)$ values of the transitions connecting states with the same single-particle components.

We mention that the $B(E2;\ 2^+ \rightarrow 0^+)$ transition strength was determined previously in a model-dependent way from a $(\mathrm{p}, \mathrm{p}')$ experiment. The obtained value of $B(E2) = 30$ W.u. [8] is much higher than that obtained from the present lifetime measurement. The origin of this discrepancy is unclear.

5.2 Octupole excitations

The coupling of the 3^- core octupole phonon to the two valence neutrons gives rise to negative-parity states. These

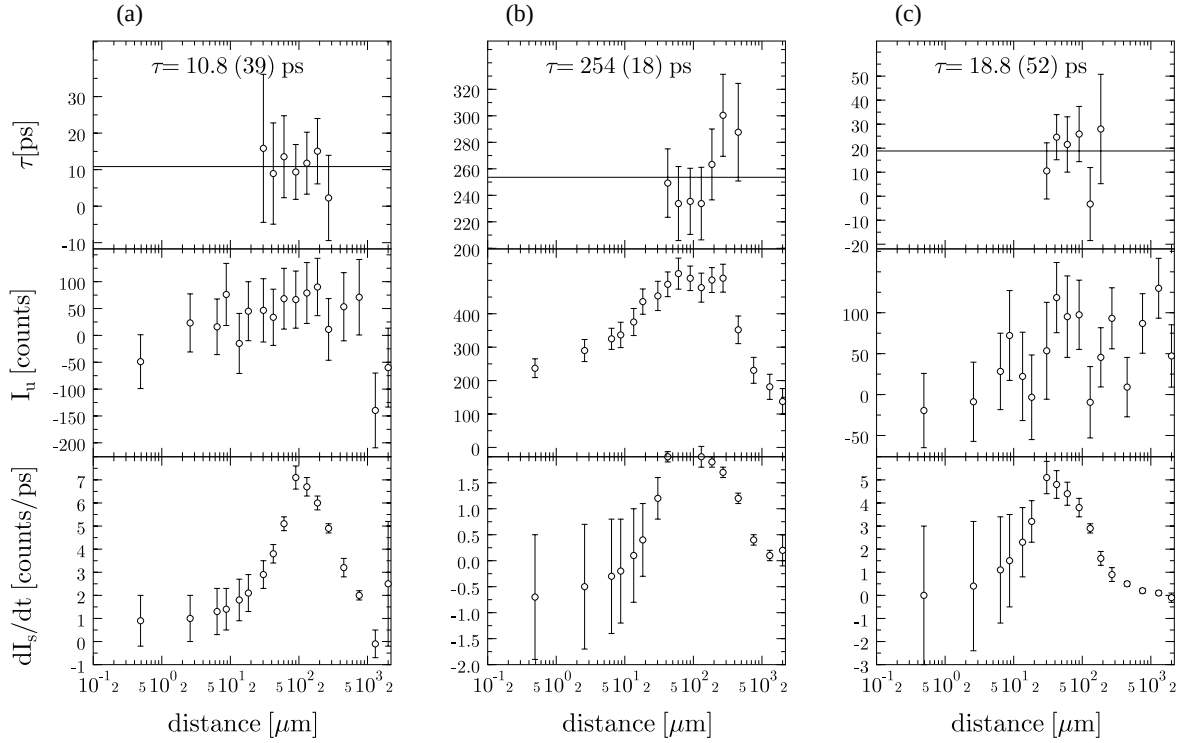

Fig. 4. Examples of lifetime analysis for the 4_1^+, 6_1^+ and 8_1^+ states (see caption of fig. 3). (a) Gate on the 395 keV $6^+ \rightarrow 4^+$ transition at 15°, analysed 632 keV at 133°; (b) gate on the 1125 keV $7^- \rightarrow 6^+$ transition at 15°, 35°, 52°, 133° and 156°, analysed 395 keV at 35°; (c) gate on the 674 keV $9^- \rightarrow 8^+$ transition at 156°, analysed 882 keV at 133°. Note that the accepted lifetimes (given in table 1) are the weighted averages of the lifetimes deduced from different ring-ring combinations.

are responsible for the yrast negative-parity levels in the second column of fig. 2. The 3^-, 5^-, 7^- and 9^- states correspond to the stretched coupling of the $(\nu f_{7/2})_{0,2,4,6}$ two neutrons to the octupole phonon. The transition strengths among these levels are $B(E2) \sim 10$ W.u., similar to those among the 0^+, 2^+, 4^+, 6^+ states having the same single-particle structure (except for the 3^- phonon). It is expected that the $B(E2;\ 11^- \rightarrow 9^-)$ strength corresponding to the $\nu h_{9/2} \rightarrow \nu f_{7/2}$ single-particle change is much lower, and similar to $B(E2;\ 8^+ \rightarrow 6^+) = 1.6$ W.u. However, the short lifetime and the low-energy feeding transition made it impossible to obtain an informative $B(E2)$ value from the present experiment. Based on shell model calculations [3], the 1913 keV 4^- and 3030 keV 8^- levels were interpreted as $I_{\max} - 1$ states, $(\nu f_{7/2})_2 \otimes 3^-$ and $(\nu f_{7/2})_6 \otimes 3^-$, respectively. The configuration assignment of the 4^- state is supported by the large $M1$ strength, $B(M1) = 0.6(3)$ W.u. of the transition connecting the $I_{\max} = 5$ level to this state. Although we favour the octupole character assignment to the 3030 keV level, the situation in this case is somewhat less clear. This level decays into the 9^- and 7^- states with the same single-particle components via weak $M1$ transitions $B(M1) \sim 2$–5×10^{-3} W.u. The other close-lying 8^- state at 3153 keV has a similar decay pattern (although the transition strengths were not determined). Therefore, these two states may be strongly mixed, both with significant octupole components. Both 8^- states are fed by $M1$ transitions from the 9^- 3368 keV level of $(\pi h_{11/2} g_{7/2}^{-1})(\nu f_{7/2}^2)_0$ configuration, and by $E2$ transitions from the 10^- 3919 keV $(\pi h_{11/2} d_{5/2}^{-1})_8 (\nu f_{7/2}^2)_2$ (see sect. 5.4). The weaker connections, both $M1$ and $E2$, of the 3030 keV state to the feeder 9^- and 10^- states favours the adopted configuration assignment.

The 3981 keV 12^+ state is interpreted as a two–octupole-phonon state, with two 3^- phonons coupled to the $(\nu f_{7/2}^2)_{6^+}$ two-neutron configuration. The determined lifetime, $\tau = 88(9)$ ps, is in agreement with the formerly measured value [6], and it is more accurate. A detailed discussion of this state together with the 9^- and 3^- one-octupole states, with special emphasis on the $B(E3)$ octupole transition strengths, has already been published elsewhere [7].

The 10^+ state at 3823 keV was interpreted as a two–octupole-phonon state, based on shell model calculations [3]. The low strength of the feeding 678 keV $E2$ transition, from the 12^+ $(\pi h_{11/2}^2)_{10} (\nu f_{7/2}^2)_2$ configuration (see sect. 5.4 below) is in agreement with this assignment.

5.3 Proton particle-hole two-neutron states

The negative-parity states of the third column of fig. 2. are formed by proton particle-hole excitations with the

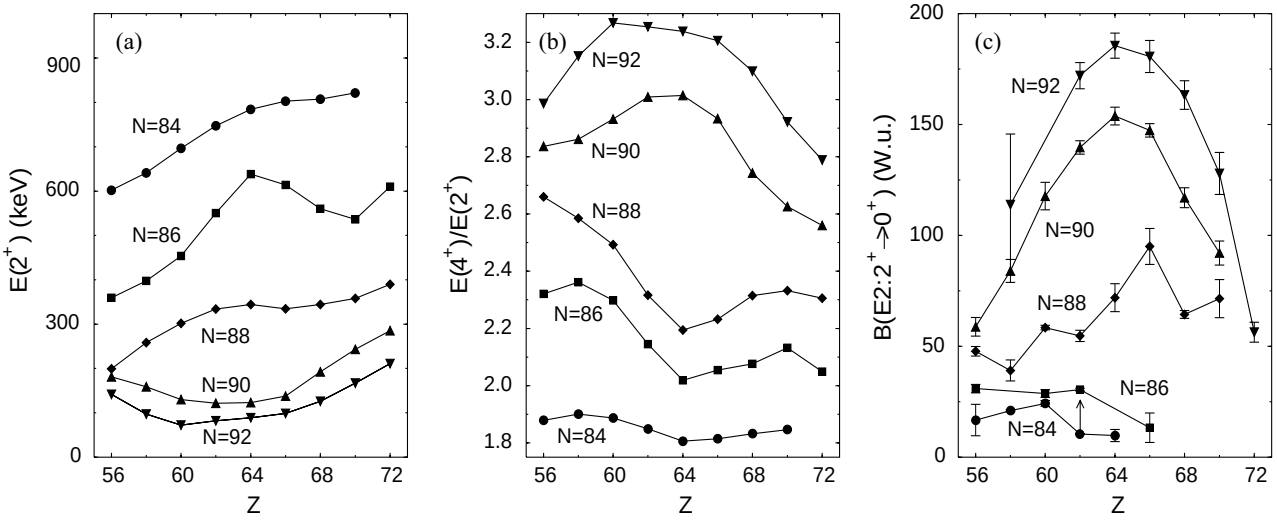

Fig. 5. Systematics of the (a) $E(2_1^+)$ energies, (b) $E(4_1^+)/E(2_1^+)$ energy ratios and (c) $B(E2:2^+ \rightarrow 0^+)$ reduced transition strengths in the vicinity of the $Z = 64$ proton number, for nuclei with $N > 82$. The data were taken from the corresponding electronic Nuclear Data Sheets compilations [15].

particle in $\pi h_{11/2}$ and the hole in either $\pi d_{5/2}$ or $\pi g_{7/2}$, and two neutrons in $\nu f_{7/2}$.

From comparison with the ^{146}Gd core nucleus, the $(\pi h_{11/2} g_{7/2}^{-1})(\nu f_{7/2}^2)_0$ character for the 3368 keV 9^- and 3311 keV 8^- states, and the $(\pi h_{11/2} d_{5/2}^{-1})(\nu f_{7/2}^2)_0$ character for the 8^- 3153 keV and 7^- 2937 keV states were suggested [3]. Our lifetime results support this interpretation. The strength of the $E2$ transition connecting the mentioned 9^- and 7^- levels, $B(E2;\ 431\ \text{keV}) = 2(1)$ W.u., is typical for a single-particle change in configuration. As mentioned before, the 3153 keV and 3030 keV 8^- states are strongly mixed, both having similar feeding and decay patterns. Since the 9^- state populates the 3030 keV state with higher strength, four times higher compared to the other 8^- state, we favour the $(\pi h_{11/2} d_{5/2}^{-1})(\nu f_{7/2}^2)_0$ main character for the 3153 keV level.

The 9^- $(\pi h_{11/2} g_{7/2}^{-1})(\nu f_{7/2}^2)_0$ state is fed by a cascade of quadrupole transitions with energies of 754, 430 and 566 keV. The large reduced strength of these transitions, $B(E2) \sim$10 W.u., suggests a $(\pi h_{11/2} g_{7/2}^{-1})(\nu f_{7/2}^2)_{2,4,6}$ character for the 11^-, 13_1^-, 15^- states of column three. The configuration assignment of the 13_2 state and of the even-spin 10^-, 12^- and 14^- levels is more difficult. Probably, the mixing of the $(\pi h_{11/2} g_{7/2}^{-1})_8(\nu f_{7/2}^2)_{2,4,6}$ and $(\pi h_{11/2} d_{5/2}^{-1})_8(\nu f_{7/2}^2)_{2,4,6}$ configurations is large. The low strengths of the 766 keV $E2$ and 551 keV $M1$ transitions connecting the 10^- state to the $(\pi h_{11/2} d_{5/2}^{-1})_8$ and $(\pi h_{11/2} g_{7/2}^{-1})_9$ levels, $B(E2) = 2.6(5)$ W.u. and $B(M1) = 2.0(4)\times10^{-3}$ W.u., respectively, suggest a different single-particle composition in the 10^- state; therefore the $(\pi h_{11/2} g_{7/2}^{-1})_8(\nu f_{7/2}^2)_2$ character is favoured.

We mention the cascade of strong $M1$ transitions connecting the $15^- \rightarrow 14^- \rightarrow 13_1^- \rightarrow 12^- \rightarrow 11^-$ states, all with strength larger than 10^{-2} W.u. This is characteristic for transitions connecting states with the same single-particle structure. In contrast, the $M1$ transitions connecting states with different character are much weaker.

5.4 Two-proton two-neutron states

The positive-parity states on the right-hand side of fig. 2. have four-particle character. The 10^+, 12^+, 14^+, 16^+ states are formed by coupling the two neutrons $(\nu f_{7/2}^2)_{0,2,4,6}$ to the fully aligned $(\pi h_{11/2}^2)_{10}$ proton pair. All the $E2$ transitions connecting these states have a strength of $B(E2) \sim$ 10 W.u., similar to the other $(\nu f_{7/2}^2)_I \rightarrow (\nu f_{7/2}^2)_{I-2}$ transitions in this nucleus. The 18^+ state is formed by lifting one neutron to the $h_{9/2}$ orbital. Due to the low-production cross-section of this high-spin state, no lifetime data could be extracted using the coincidence DDCM. Only a lifetime limit of $\tau < 0.6$ ns could be obtained, by gating from below, which leads to a poorly determined $B(E2)$ transition strength limit. The direct feeding of the 18^+ state by a 20^- $\tau = 2$ ns isomer [3] explains the long effective lifetime. We note the presence of two 10^+ states very close to each other in the level scheme, at 3759 and 3823 keV, respectively. Both of these are fed from the 12^+ state. The adopted configuration assignment, as shown in fig. 2, is based on the large $B(E2;\ 742\ \text{keV}) = 6(3)$ W.u. strength.

5.5 Z = 64 subshell closure and the B(E2 : $2^+ \rightarrow 0^+$) systematics

It is well established that for neutron number close to $N = 82$, a subshell closure is present for proton number $Z = 64$. This is reflected by the systematics of the $E(2^+)$ energy and the $E(4^+)/E(2^+)$ ratio (see fig. 5). On the other hand, for rare-earth nuclei with $N \geq 88$ a maximum

of the deformation is reached just at $Z = 64$ [14]. In fact, the $B(E2)$ values of the $2^+ \rightarrow 0^+$ transitions are highest at $Z = 64$ for nuclei above $N = 88$ (see fig. 5). For nuclei with $N = 84$, where the $Z = 64$ shell closure still acts, we should observe a minimum of the $E2$ strength of the $2^+ \rightarrow 0^+$ transition. Indeed, the new experimental point obtained in the present work for ^{148}Gd is the lowest along the $N = 84$ chain (see fig. 5c) and confirms therefore, through the more stringent test of a $B(E2)$ measurement, the double-shell closure at $N = 82$ and $Z = 64$.

6 Conclusions

The lifetimes of more than 20 excited states in ^{148}Gd were measured in a coincidence plunger experiment. Based on the deduced transition strengths, unambiguous configuration assignments could be given for almost all the populated levels. The proposed assignments are in good agreement with previous shell model calculations [3]. The $B(E2 : 2^+ \rightarrow 0^+)$ has its smallest value in ^{148}Gd among the $N > 82$ nuclei in the region.

The authors thank the staff of the XTU Tandem of LNL for the stable operation of the accelerator. We are grateful for Prof. P.M. Walker for useful discussions. This work has been supported by the European Comission through Contract No. ERBFMCT980119 E.U. TMR Program. Zs.P. acknowledges receipt of an EPSRC Advanced Fellowship Award (GR/A10789/01).

References

1. P. Kleinheinz, R. Broda, P.J. Daly, S. Lunardi, M. Ogawa, J. Blomqvist, Z. Phys. A **290**, 279 (1979).
2. S. Lunardi, P. Kleinheinz, M. Piiparinen, M. Ogawa, M. Lach, J. Blomqvist, Phys. Rev. Lett. **53**, 1531 (1984).
3. M. Piiparinen, P. Kleinheinz, S. Lunardi, M. Ogawa, G. de Angelis, F. Soramel, W. Meczynski, J. Blomqvist, Z. Phys. A **337**, 387 (1990).
4. M.W. Drigert, M. Piiparinen, R.V.F. Janssens, R. Holzmann, I. Ahmad, J. Borggreen, R.R. Chasman, P.J. Daly, B.K. Dichter, H. Emling, U. Garg, Z.W. Grabowski, T.L. Khoo, W.C. Ma, M. Quader, D.C. Radford, W. Trzaska, Nucl. Phys. A **515**, 466 (1990).
5. O. Häusser, P. Taras, W. Trautmann, D. Ward, T.K. Alexander, H.R. Andrews, B. Haas, D. Horn, Phys. Rev. Lett. **42**, 1451 (1979).
6. M. Piiparinen, P. Kleinheinz, J. Blomqvist, A. Virtanen, A. Atac, D. Muller, J. Nyberg, T. Ramsoy, G. Sletten, Phys. Rev. Lett. **70**, 150 (1993).
7. Zs. Podolyák, P.G. Bizzeti, A.M. Bizzeti-Sona, S. Lunardi, D. Bazzacco, A. Dewald, A. Algora, G. de Angelis, M. De Poli, E. Farnea, A. Gadea, D.R. Kasemann, T. Klug, Th. Kröll, S. Lenzi, D.R. Napoli, C.M. Petrache, R. Peusquens, C. Rossi Alvarez, T. Martinez, C.A. Ur, Eur. Phys. J. A **8**, 147 (2000).
8. G. de Angelis, P. Kleinheinz, B. Rubio, J.L. Tain, K. Zuber, B. Brinkmöller, P. von Rossen, J. Römer, D. Paul, J. Meissburger, G.P.A. Berg, A. Magiera, G. Hlawatsch, L.G. Mann, T.N. Massey, D. Decman, G.L. Struble, J. Blomqvist, Z. Phys. A **336**, 375 (1990).
9. M.R. Bhat, Nucl. Data Sheets **89**, 797 (2000).
10. A. Dewald, P. Sala, R. Wrzal, G. Böhm, D. Lieberz, G. Siems, R. Wirowski, K.O. Zell, A. Gelberg, P. von Brentano, P. Nolan, A.J. Kirwan, P.J. Bishop, R. Julin, A. Lampinen, J. Hattula, Nucl. Phys. A **545**, 822 (1992).
11. C. Rossi Alvarez, in *XVI Nuclear Physics Divisional Conference Structure of Nuclei Under Extreme Conditions SNEC98, Padova, March 31-April 4, 1998*, Nuovo Cimento A **111**, 601 (1998).
12. A. Dewald, S. Harissopulos, P. von Brentano, Z. Phys. A **334**, 163 (1989).
13. G. Böhm, A. Dewald, P. Petkov, P. von Brentano, Nucl. Instrum. Methods Phys. Res. A **329**, 248 (1993).
14. R.F. Casten, D.D. Warner, D.S. Brenner, R.L. Gill, Phys. Rev. Lett. **47**, 1433 (1981).
15. Nuclear Structure and Decay Data, National Nuclear Data Center, Brookhaven National Laboratory, at `http://www.nndc.bnl.gov/nndc`.